energies

MDPI

Article

Optimal Magnetic Field Shielding Method by Metallic Sheets in Wireless Power Transfer System

Feng Wen and Xueliang Huang *

School of Electrical Engineering, Southeast University, No. 2 Sipailou, Nanjing 210096, China; wf133@163.com
* Correspondence: xlhuang@seu.edu.cn; Tel.: +86-25-8379-2260

Academic Editor: Sheldon S. Williamson
Received: 3 July 2016; Accepted: 6 September 2016; Published: 9 September 2016

Abstract: To meet the regulations established to limit human exposure to time-varying electromagnetic fields (EMFs) such as the International Committee on Non-Ionizing Radiation Protection (ICNIRP) guidelines, thin metallic sheets are often used to shield magnetic field leakage in high power applications of wireless power transfer (WPT) systems based on magnetic field coupling. However, the metals in the vicinity of the WPT coils cause the decrease of self and mutual inductances and increase of effective series resistance; as such, the electric performance including transmission power and the efficiency of the system is affected. With the research objective of further investigating excellent shielding effectiveness associated with system performance, the utilization of the optimal magnetic field shielding method by metallic sheets in magnetic field coupling WPT is carried out in this paper. The circuit and 3D Finite Element Analysis (FEA) models are combined to predict the magnetic field distribution and electrical performance. Simulation and experiment results show that the method is very effective by obtaining the largest possible coupling coefficient of the WPT coils within the allowable range and then reducing the value nearest to and no smaller than the critical coupling coefficient via geometric unbroken metallic sheets. The optimal magnetic field shielding method which considers the system efficiency, transmission power, transmission distance, and system size is also achieved using the analytic hierarchy process (AHP). The results can benefit WPT by helping to achieve efficient energy transfer and safe use in metal shielded equipment.

Keywords: wireless power transfer (WPT); magnetic field coupling; metallic sheets; analytic hierarchy process (AHP)

1. Introduction

Wireless power transfer (WPT) technology using magnetic field coupling, offering wireless mid-range power transmission, has been used for a variety of applications, such as implantable biomedical devices, mobile electronics, household appliances, and electric vehicles [1–4]. However, as the WPT technology is becoming more widely used in high power applications, human exposure to time-varying electromagnetic fields (EMFs) accordingly increases. As a result, internal electric fields inducing body currents in tissues can end up stimulating the nervous system, depending on the frequency involved. Thus, magnetic field leakage from WPT systems should be suppressed and comply with the related regulations to make the WPT technology safe and accessible. By attaching shielding materials, such as aluminum sheets, exposure levels can be controlled by a canceling magnetic field produced by the induced eddy currents on the metal face [5–7]. However, the parameters of the WPT system are also influenced by the metallic sheets that are in a close proximity. Research on the electric performance of WPT systems has been conducted. To enhance the magnetic coupling, a ferrite plate or sheet is typically employed and located between the coil and the metal plate [8]. However, the magnetic materials will also bring in disadvantages in size, weight, and cost, and result in sizeable power losses in high frequency and power applications. The transfer efficiency can be optimized and

the position error tolerance can be improved by placing two metallic sheets symmetrically behind the driving and pick-up coils [9,10]. This approach is restricted by several complicated factors, such as the system size, variable coupling conditions, and the structure of the metallic sheets in a practical implementation. Therefore, further research should be carried out on optimal magnetic field shielding methods that consider the shielding effectiveness associated with the electric performance, and other characteristics such as transmission distance and system size.

In this paper, we study the effects and system performance of shielding materials on the magnetic field from a magnetic field coupling WPT system. The circuit and 3D Finite Element Analysis (FEA) models are combined to predict the magnetic field distribution and electrical performance. By varying the geometric configuration of the metallic sheets and the coupling condition of the WPT coils, the metal shielding effectiveness is investigated. Using the analytic hierarchy process (AHP), an optimal magnetic field shielding method that considers the system efficiency, transmission power, transmission distance, and system size is also achieved.

2. Analysis Models and Methods

The modelization of a magnetic field coupling WPT system for predicting the magnetic field in the surrounding region is not a trivial issue. Actually, the currents in the coils are unknown and detailed multi-turn coils modeling in complex vicinal environments is difficult due to high memory storage and computer time requirements. Meanwhile, the inclusion of circuit terminal conditions at some ports coincident with the coils' terminals can significantly increase the computational cost. To overcome the inconvenience, the following three-step approach can be used:

First, the electric parameters are extracted by the electromagnetic (EM) field solver;

Then, the currents flowing in the coils are calculated by the circuit approach;

Finally, the obtained currents are used as the source of the magnetic field which is calculated by the EM field solver.

2.1. Circuit Model

The equivalent circuit model of the WPT system under the influence of metallic objects based on mutual inductance theory is shown in Figure 1. There, L_1, L_2, L_3, and L_4 are the self-inductance of the driving, transmission, receiving, and pick-up coils, respectively, C_1, C_2, C_3, and C_4 the respective resonance capacitance of the coils, R_1, R_2, R_3, and R_4 the equivalent resistances of the coils, R_p the internal resistance of the power supply (50 Ω), R_L the load resistance (50 Ω), and V_1 the excitation voltage source. The metals can be treated as an equivalent resistor R_A, connected with a serial equivalent inductor L_A [11–13]. M_{mn} are the mutual inductance of any pair of coils and metals, with $m, n \in \{1, 2, 3, 4, A\}$.

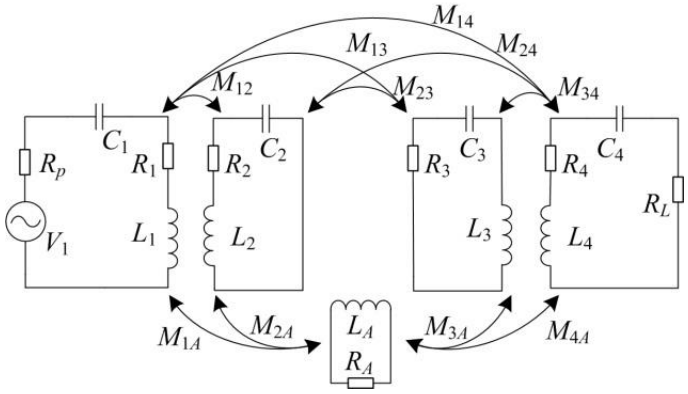

Figure 1. Equivalent circuit model of the wireless power transfer (WPT) system under the influence of metallic objects.

According to Kirchhoff's law, the impedance matrix of the system while the electric parameters of metallic sheets are mapped into the coils can be expressed as

$$\begin{bmatrix} Z_{11}-Z_{1A}{}^2/Z_{AA} & Z_{12}-Z_{1A}Z_{2A}/Z_{AA} & Z_{13}-Z_{1A}Z_{3A}/Z_{AA} & Z_{14}-Z_{1A}Z_{4A}/Z_{AA} \\ Z_{12}-Z_{1A}Z_{2A}/Z_{AA} & Z_{22}-Z_{2A}{}^2/Z_{AA} & Z_{23}-Z_{2A}Z_{3A}/Z_{AA} & Z_{24}-Z_{2A}Z_{4A}/Z_{AA} \\ Z_{13}-Z_{1A}Z_{3A}/Z_{AA} & Z_{23}-Z_{2A}Z_{3A}/Z_{AA} & Z_{33}-Z_{3A}{}^2/Z_{AA} & Z_{34}-Z_{3A}Z_{4A}/Z_{AA} \\ Z_{14}-Z_{1A}Z_{4A}/Z_{AA} & Z_{24}-Z_{2A}Z_{4A}/Z_{AA} & Z_{34}-Z_{3A}Z_{4A}/Z_{AA} & Z_{44}-Z_{4A}{}^2/Z_{AA} \end{bmatrix} \cdot \begin{bmatrix} I_1 \\ I_2 \\ I_3 \\ I_4 \end{bmatrix} = \begin{bmatrix} V_1 \\ 0 \\ 0 \\ 0 \end{bmatrix} \quad (1)$$

where $Z_{nn} = R_{nn} + jX_{nn}$, $Z_{mn} = jX_{mn}$, $X_{mn} = \omega M_{mn}$, $m, n \in \{1, 2, 3, 4, A\}$, $X_{nn} = \omega L_n - 1 / (\omega C_n)$, $n \in \{1, 2, 3, 4\}$, $R_{11} = R_p + R_1$, $R_{22} = R_2$, $R_{33} = R_3$, $R_{44} = R_L + R_4$, $R_{AA} = R_A$, $X_{AA} = \omega L_A$. V_1 is the root mean square (RMS) value of the excitation voltage source. I_1, I_2, I_3, and I_4 are RMS values of the currents in the coils and can be calculated using Equation (1).

The transmission power of the WPT system provided by the pick-up coil can be written as

$$P_o = |I_4|^2 \cdot R_L \quad (2)$$

The input power of the system excluding the power resistance loss can be expressed by

$$P_{in} = \mathrm{Re}[(V_p - R_p \cdot I_1) \cdot I_1{}^*] \quad (3)$$

The system efficiency can be calculated using

$$\eta = P_o / P_{in} \quad (4)$$

2.2. FEA Model

Figure 2 depicts the geometry of metallic plates in the presence of WPT coils and the 3D FEA simulation model of the shielded coil structure for a WPT system. The four WPT coils are 25 cm in radius and are wound with 0.5 cm radius copper wire. The number of turns in the driving coil (Tx Loop) and pick-up coil (Rx Loop) is one and in transmission coil (Tx Coil) and receiving coil (Rx Coil) there are five. The aluminum shielding sheets are 50 cm in radius and the thickness is 0.1 cm. The distance between the loop and the coil for both Tx and Rx is 1 cm, the loop and the sheet is d_A, and the Tx and Rx coils is d_{TR}. Along the Z axis and Y axis, where humans are usually located in WPT applications (such as the power supply for household appliances, and the battery charger for electric vehicles (EVs) or mobile electronics), the magnetic flux density are calculated. The magnetic flux density along the B field measurement line I (Z axis) and II (Y axis) can be called the vertical and the horizontal magnetic flux density, expressed by B_v and B_h, respectively.

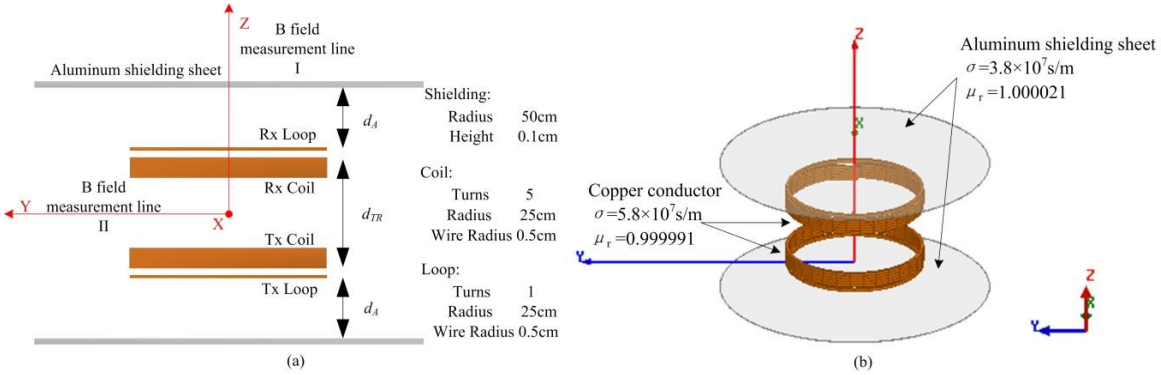

Figure 2. (**a**) Geometry of metallic sheets in the presence of WPT coils (side view); (**b**) Perspective view of Finite Element Analysis (FEA) model.

Using the FEA tool, ANSYS, the key parameters of coils without considering the aluminum shielding in Figure 2 are calculated and shown in Table 1. The coils are matched at 1 MHz by

connecting series capacitors. The coupling coefficient of the Tx Loop and Coil and the Rx Loop and Coil are denoted as k_{12}, k_{34}, respectively.

Table 1. Coil parameters without considering the metal effects.

f = 1 MHz	Self-Inductance (μH)	Resistance (mΩ)	Matched Capacitance (nF)	Coupling Coefficient
Tx Loop	1.196	12.316	21.170	k_{12} = 0.608
Tx Coil	21.938	106.660	1.155	
Rx Coil	21.938	104.233	1.155	k_{34} = 0.607
Rx Loop	1.197	12.126	21.154	

3. Metal Shielding Effectiveness

3.1. Metal Shielding Work and Failure

Within a conductive material exposed to a time-varying magnetic field, eddy currents are induced. These circulating eddies of current have inductance and induce magnetic fields. These fields cancel the incident magnetic fields penetrating the material, and so the net magnetic field in the vicinity of the material is reduced [14]. Obviously, the distribution of the eddy currents flowing in certain geometric configuration might be the key in the metal shielding effect and therefore needs to be researched.

With the purpose of figuring out the eddy currents distribution in the metal, as well as the aim of achieving an optimized geometric configuration, we etch n number of slots on both of the two aluminum sheets, as shown in Figure 3, to study the change in eddy currents distribution with the metal geometric. All the slots are 45cm length from the edge to the center with s width and 0.1 cm deep.

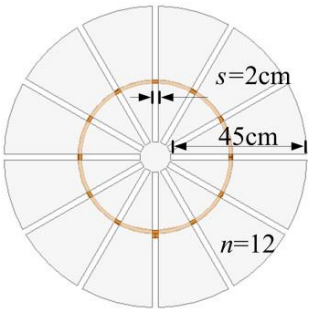

Figure 3. Slots on aluminum sheet.

While P_o = 3 kW, $\omega = 2 \times \pi \times 10^6$ rad/s, and the variable values in Figure 2 are substituted as d_{TR} = 60 cm, d_A = 10 cm, the impedance matrix in Equation (1) can be obtained using ANSYS, the currents in the coils can be calculated using Equations (1) and (2) and the magnetic flux and eddy currents density on aluminum sheet above the Rx Loop are presented in Figure 4. Figure 4a, c show that the magnetic flux density and eddy currents density are weak on the upper surface of unslotted aluminum sheet. It can be observed from Figure 4b, d that the magnetic flux density is high on the lower surface of the unslotted aluminum sheet edge and the region close to the coils, and the eddy currents also concentrate close to the high-intensity magnetic field region. The magnetic field and eddy currents distribution on the slotted aluminum sheet are presented in Figure 4e–h where n = 12 and s = 2 cm. We can see that the slots cut through what were originally high-intensity magnetic field regions on the sheet where the eddy currents are supposed to be high. As a result, relatively stronger eddy currents flow along the edges of the slots on both the upper surface and the lower surface while the weaker currents flow on partitions segmented by slots. Although the eddy currents density J A/m^2 is strong on the edges of the slots, total currents I (A) won't be high due to the weak eddy currents density on most of the area of the sheet. The eddy currents on unslotted sheet are much

larger than that on the slotted sheet, as Figure 4d,g,h show; thus the induced magnetic field by the eddy currents on the unslotted sheet is obviously stronger. The eddy currents' redistribution leads to the variation in the magnetic field. By comparing the magnetic flux density on the upper surface in Figure 4a,e, the unslotted sheet might show better shielding effectiveness. We can conclude that slots on the metallic sheets can distinctly change the eddy currents distribution, and the metallic sheets' geometric configuration might be extremely relevant to its shielding effect.

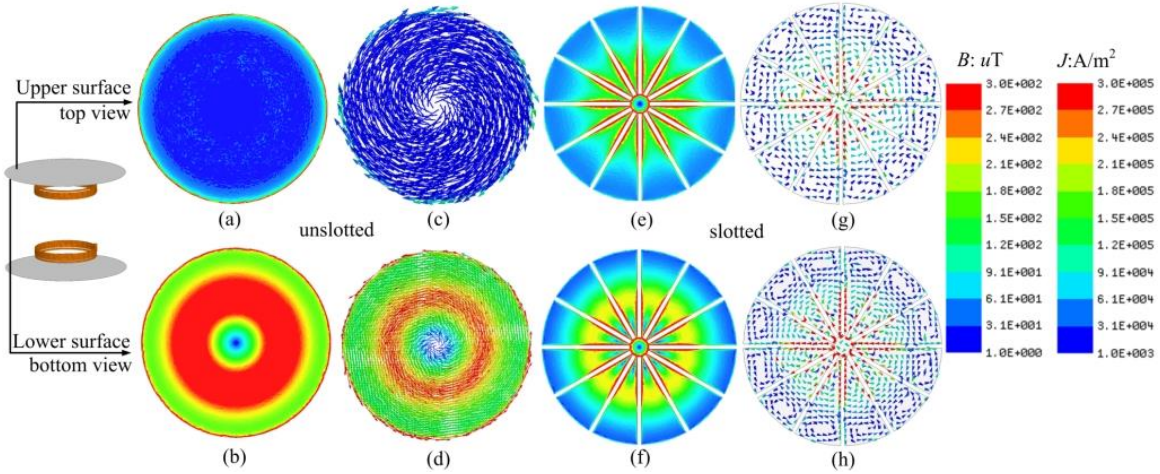

Figure 4. Magnetic flux density on an unslotted aluminum sheet: (**a**) on the upper surface; (**b**) on the lower surface; Eddy currents density on an unslotted aluminum sheet: (**c**) on the upper surface; (**d**) on the lower surface; Magnetic flux density on a slotted aluminum sheet: (**e**) on the upper surface; (**f**) on the lower surface; Eddy currents density on a slotted aluminum sheet: (**g**) on the upper surface; (**h**) on the lower surface.

Various slots' number n and width s are analyzed in Figure 5 as the excitation voltage source V_1 = 1 kV. The impedance matrix of the WPT system with slotted aluminum sheets can be obtained by ANSYS. Using Equations (1), (2) and (4), the efficiency of system η can be calculated as 95.65% with none shielding and 63.98% with unslotted aluminum sheets, the transmission power P_o 4.15 kW and 0.06 kW, respectively, with the increase of n and s, η and P_o will increase close to none shielding condition on account of the decrease of eddy currents.

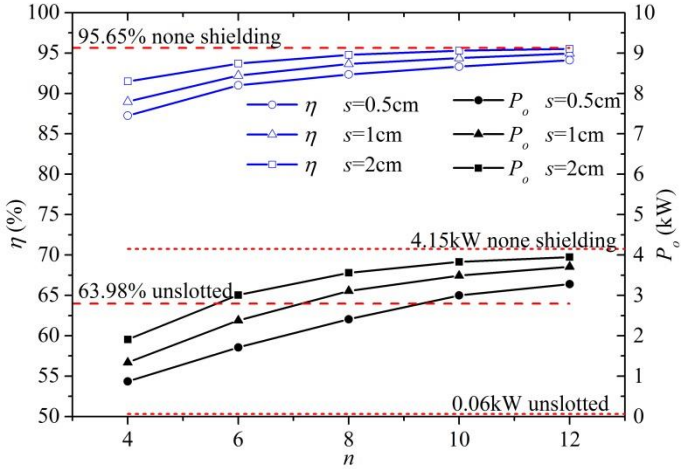

Figure 5. Results of η and P_o for different slots in Figure 4 under constant excitation voltage of 1 kV.

In order to compare the differences in the vertical magnetic flux density B_v under the condition of constant transmission power P_o of 3 kW, the simulated results along the measure line I are shown

in Figure 6a with human exposure limits published by the International Committee on Non-Ionizing Radiation Protection (ICNIRP) [15,16]. The graphed contours shown in Figure 6a clearly illustrate the differences in each magnetic flux density distribution. In particular, the unslotted aluminum sheets significantly shield the magnetic field in a wide range away from Z = 40 cm where the upper aluminum sheet locates while the slotted one can only reduce the magnetic flux density within an extremely narrow range close to the aluminum sheet, and more slots will lead to a weaker shielding effect. Figure 6b shows the differences of magnetic field distribution on XY plane with various Z values between the none shielding condition and the slotted one. The eddy currents on the slotted sheet will strengthen magnetic field in the immediate vicinity to the slots, the magnetic field distribution approximates to a none shielding condition and the slotted sheet shows little shielding effect beyond a small distance due to the weak total eddy currents on the slotted sheet.

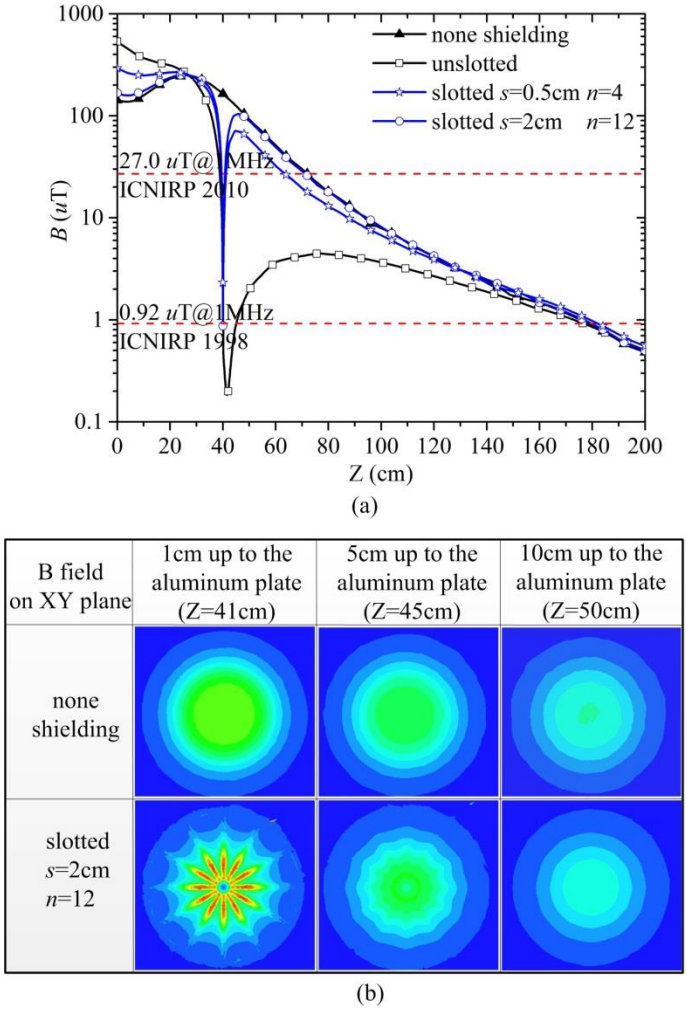

Figure 6. (**a**) B_v under the condition of constant transmission power of 3 kW; (**b**) Magnetic field distribution on XY plane.

According to the above conclusion, the aluminum sheet with the slots cutting through what were originally high-intensity magnetic field regions on the sheet shows a much weaker shielding effect, whereas slots in low-intensity magnetic field regions are expected to be more effective. In Figure 4b, the weak magnetic field region distributes on the center-micro-area of the sheet, so we etch this region totally as Figure 7a shows. The diameter of the circular aperture d equals 5 cm for case #1 and 10 cm for case #2. Although not as good as the unslotted condition, both the two cases show better shielding effects than the slotted ones, which can be observed by comparing the magenta curves in Figure 7b

and the blues curves in Figure 6a. The shielding effect will also decline with the increase of the circular aperture size as the high-intensity magnetic field region is etched; to improve it close to the unslotted condition, the circular aperture size should be diminished. Case #3 and case #4 are aluminum sheets with circular apertures and slots. The diameter of the aperture d is 5 cm for case #3 and 10 cm for case #4, the slots length l is 45 cm for case #3 and 40 cm for case #4. As the slots in case #3 and case #4 cut through high-intensity magnetic field regions on the sheet, the shielding effect is weakened. The efficiency of the four cases is 64.62%, 69.73%, 86.43%, and 73.16%, respectively. According to the four cases, we can conclude that better transfer efficiency is always obtained with a worse shielding effect due to the influence of eddy currents. Although the aperture size of case #4 is larger than that of case #3, case #4 shows better shielding effectiveness because of the shorter slots in high-intensity magnetic field regions. The results indicate that both the slots and aperture should be etched in weak magnetic field regions, otherwise they will lead to drastic declines in the shielding effect.

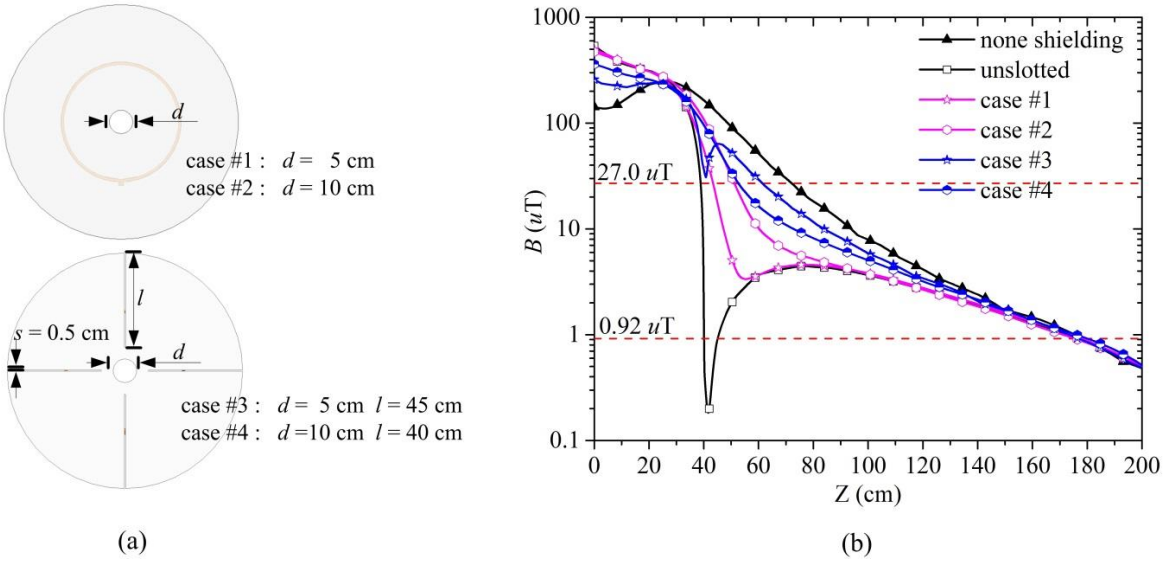

Figure 7. (**a**) Circular aperture and slots etched in aluminum sheet; (**b**) B_v under the condition of constant transmission power of 3 kW.

In summary, slots etched in the metals can alter the eddy currents path, and reduce adverse impacts on the electrical performance of a WPT system, but they might also lead to a shielding performance reduction or shielding failure. Hence, guaranteeing the integrity of the metallic sheets' geometric configuration, especially the edge and high-intensity magnetic field regions, is the key feature the metallic sheets should satisfy for demonstrating shielding effects. In addition, for the sake of achieving light-weight, economical, and small-size shielding geometric configurations within acceptable declines in the shielding effect, the metal sheets can be etched in the weak magnetic field region which varies with specific cases.

3.2. Metal Shielding Effect Contrast

In order to use metals for the suppression of magnetic field leakages from a WPT system, their effects on the electrical performance of a WPT system should be considered. The metals in the vicinity of the coils cause the decrease of self and mutual inductances and the increase of effective series resistance, as Equation (1) shows. By placing two metallic sheets symmetrically outside the Tx Loop and Rx Loop, the magnetic field can be well confined between two metallic plates, thus improving magnetic flux focusing, and the transfer efficiency of the system is also further improved [9,17]. However, this approach is often restricted by the size, structure, and variable coupling conditions, and the transmission power is also not high enough in a metal shielded environment [13]. Hence, research should be carried out on the metal shielding effect together with the electrical performance, including

the transmission power and the efficiency of the WPT system. As the previous section shows, the vertical magnetic flux density can be shielded effectively by aluminum sheets, however, the horizontal magnetic flux density must be studied to achieve the optimal shielding scheme. Since the sheets used in this study are already of a suitable size, the weak magnetic field region on the sheet is so small; as such, it makes little sense to etch slots in the micro-region considering the decline in shielding effect. Thus, the geometric entirely unbroken metallic sheets are adopted for further research for purposes of simplicity.

According to the impedance matrix in Equation (1), we define the coupling coefficient of the Tx and Rx Coils in consideration of the metal effects as

$$k_{23}{}^{A} = \frac{\mathrm{Im}[Z_{23} - Z_{2A}Z_{3A}/Z_{AA}]}{\sqrt{\mathrm{Im}[j\omega L_2 - Z_{2A}{}^2/Z_{AA}] \cdot \mathrm{Im}[j\omega L_3 - Z_{3A}{}^2/Z_{AA}]}} \tag{5}$$

The critical coupling coefficient [18] without considering the metal effects can be calculated using

$$k_c = \sqrt{\frac{(Z_{12}{}^2/R_{11} + R_{22})^2 + (Z_{34}{}^2/R_{44} + R_{33})^2}{2\omega^2 L_2{}^2}} \tag{6}$$

The critical coupling coefficient of the WPT coils in Figure 2 equals 0.056 using Equation (6) with the parameters in Table 1. Different values of d_{TR} and d_A are set to the research variable coupling conditions of the WPT coils. Coupling coefficient $k_{23}{}^{A}$ is shown in Table 2, the results of η and P_o as V_1 = 1 kV, $\omega = 2 \times \pi \times 10^6$ rad/s are shown in Figure 8. The values in Table 2 indicate that the coupling coefficient of the Tx and Rx Coils in consideration of the metal effects $k_{23}{}^{A}$ will increase close to none shielding value k_{23} with the increase of the sheets distance d_A.

Table 2. Coupling coefficient with and without considering the metal effects.

Coupling Coefficient	d_{TR} = 30 cm	d_{TR} = 45 cm	d_{TR} = 60 cm
$k_{23}{}^{A}$ (d_A = 10 cm)	0.124	0.047	0.021
$k_{23}{}^{A}$ (d_A = 20 cm)	0.152	0.062	0.029
$k_{23}{}^{A}$ (d_A = 30 cm)	0.164	0.068	0.033
$k_{23}{}^{A}$ (d_A = 40 cm)	0.169	0.072	0.035
$k_{23}{}^{A}$ (d_A = 50 cm)	0.171	0.073	0.036
$k_{23}{}^{A}$ (d_A = 60 cm)	0.172	0.074	0.036
k_{23} (none shielding)	0.173	0.075	0.037

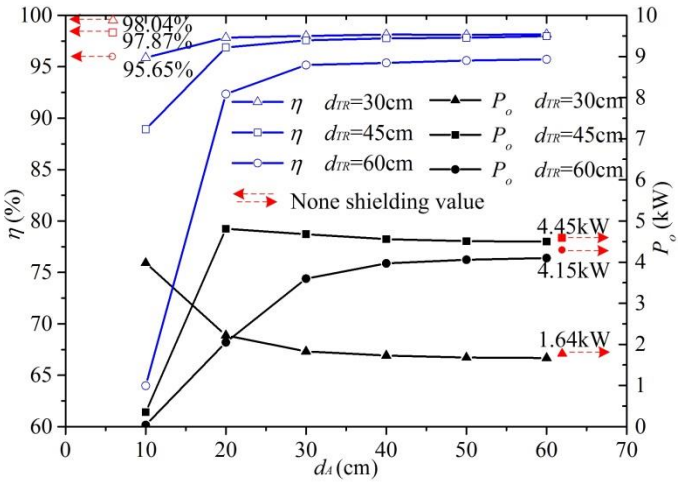

Figure 8. Results of η and P_o for various coupling conditions under the constant excitation voltage of 1 kV.

As the curves in Figure 8 show, when d_{TR} = 30 cm (k_{23} = 0.173), P_o = 1.64 kW, and η = 98.04%, as d_A increases from 10 cm to 60 cm, P_o decreases from 3.98 kW to 1.67 kW, and η increases from 95.89% to 98.16%; when d_{TR} = 45 cm (k_{23} = 0.075), P_o = 4.45 kW and η = 97.87%; as d_A = 10 cm, P_o = 0.35 kW and η = 88.92%; as d_A = 20 cm, P_o = 4.81 kW and η = 96.88%; as d_A increases to 60 cm, P_o decreases to 4.50 kW and η increases to 97.98%; when d_{TR} = 60 cm (k_{23} = 0.037), P_o = 4.15 kW, η = 95.65%, as d_A increases from 10 cm to 60 cm, P_o increases from 0.06 kW to 4.10 kW and η increases from 63.98% to 95.73%.

We can summarize from Table 2 and Figure 8:

- The coupling coefficient of the coils changes based upon the metallic sheets in the vicinity and the transmission power P_o reaches peak as the coupling coefficient of the coils (k_{23}, ${k_{23}}^A$) approaches the critical coupling coefficient k_c;
- P_o decreases to a stable value gradually with the increase of ${k_{23}}^A$ when ${k_{23}}^A > k_c$; P_o decreases to zero rapidly with the decrease of ${k_{23}}^A$ when ${k_{23}}^A < k_c$;
- The efficiency of system η increases with ${k_{23}}^A$ and has a slight improvement against the none shielding condition when ${k_{23}}^A$ is large; η decreases drastically when ${k_{23}}^A$ is small.

The horizontal magnetic flux density B_h under the condition of constant transmission power P_o of 3 kW along the measure line II is shown in Figure 9.

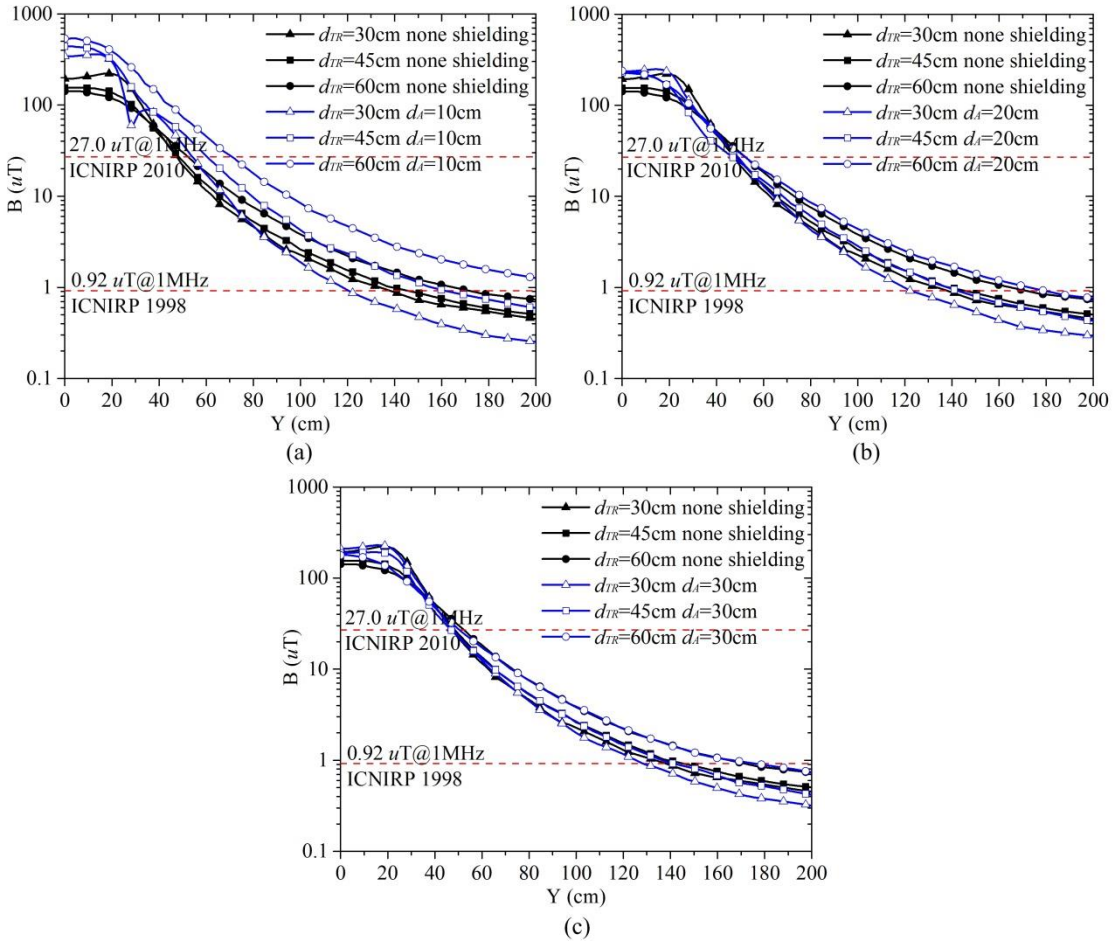

Figure 9. B_h under the condition of constant transmission power of 3 kW. (**a**) d_A = 10 cm. (**b**) d_A = 20 cm. (**c**) d_A = 30 cm.

In the range 100 cm $\leq$ Y $\leq$ 200 cm, none shielding curves in Figure 9 show

$$B_{d_{TR}=60cm} > B_{d_{TR}=45cm} > B_{d_{TR}=30cm} \quad (7)$$

By contrasting the aluminum shielding and none shielding curves in Figure 9a–c, respectively, we can get

$$\Delta B_{d_{TR}=60cm,d_A=10cm} > \Delta B_{d_{TR}=45cm,d_A=10cm} > 0 > \Delta B_{d_{TR}=30cm,d_A=10cm} \quad (8a)$$

$$\Delta B_{d_{TR}=60cm,d_A=20cm} > 0 > \Delta B_{d_{TR}=45cm,d_A=20cm} > \Delta B_{d_{TR}=30cm,d_A=20cm} \quad (8b)$$

$$\Delta B_{d_{TR}=60cm,d_A=30cm} > 0 > \Delta B_{d_{TR}=45cm,d_A=30cm} > \Delta B_{d_{TR}=30cm,d_A=30cm} \quad (8c)$$

By comparing curves in Figure 9, we can also get

$$0 > \Delta B_{d_{TR}=30cm,d_A=30cm} > \Delta B_{d_{TR}=30cm,d_A=20cm} > \Delta B_{d_{TR}=30cm,d_A=10cm} \quad (9a)$$

$$\Delta B_{d_{TR}=45cm,d_A=10cm} > 0 > \Delta B_{d_{TR}=45cm,d_A=30cm} > \Delta B_{d_{TR}=45cm,d_A=20cm} \quad (9b)$$

$$\Delta B_{d_{TR}=60cm,d_A=10cm} > \Delta B_{d_{TR}=60cm,d_A=20cm} > \Delta B_{d_{TR}=60cm,d_A=30cm} > 0 \quad (9c)$$

where ΔB is the difference in value of the magnetic flux density between the aluminum shielding condition and none shielding condition. In Figure 9, the safe region meeting the ICNIRP 1998 guidelines is largest as d_{TR} = 30 cm and d_A = 10 cm.

Figure 10 shows the magnetic field distribution on a YZ plane under various coupling conditions.

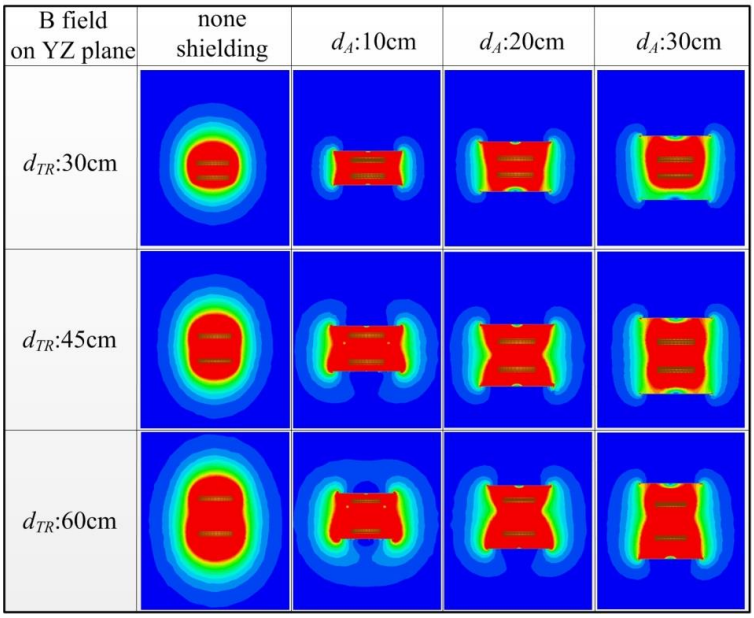

Figure 10. Magnetic field distribution on a YZ plane.

We can reach the following conclusions from Figures 9 and 10:

- Metallic sheets can shield the vertical magnetic field well, but are relatively weak at shielding the horizontal magnetic field;
- In the condition of none metal shielding and constant transmission power P_o, the larger the coupling coefficient of the coils k_{23} is, the weaker the horizontal magnetic field will be. B_h increases rapidly with the decrease of k_{23} when $k_{23} < k_c$, and decreases slowly with the increase of k_{23} when $k_{23} > k_c$;
- In the metal shielding condition, the horizontal magnetic field is stronger than the none shielding condition when $k_{23}{}^A < k_c$. The metallic sheets show no shielding effect; this is because the metallic sheets in the vicinity of the coils under a low coupling coefficient will seriously affect the transmission characteristics of the WPT system, and therefore more input current is needed to keep the transmission power constantly. The smaller $k_{23}{}^A$ is, the larger the B_h increment will

be—the increment decreases with the increase of $k_{23}{}^{A}$. As $k_{23}{}^{A} > k_c$, the increment is negative, the horizontal magnetic field is weaker than the none shielding condition, and the metallic sheets show a shielding effect. The smaller $k_{23}{}^{A}$ is, the larger B_h decrement will be.

Given the above, the metallic sheets can achieve the best shielding effect by increasing the coupling coefficient of the coils k_{23} as large as possible within the allowable range and by utilizing the metal effects to make $k_{23}{}^{A}$ nearest to and no smaller than k_c: $k_{23}{}^{A} - k_c \to 0^+$.

3.3. Experimental Results

To verify the above results, experimental analysis for a magnetic field coupling WPT system under the influence of metallic objects was performed. The experimental system is shown in Figure 11. In order to setup variable coupling conditions, the WPT coils and aluminum sheets were placed coaxially and were thereby able to be displaced along the Z axis. The critical coupling coefficient k_c was measured to be 0.050 and the transmission power P_o was 3 kW. The measurements of the magnetic field were taken with a PMM HP-032 (Narda, Segrate, Italy) magnetic field probe along the Y axis. The measured results are shown in Figure 12. In the none shielding condition, the larger the coupling coefficient of the coils k_{23} is, the weaker the horizontal magnetic field will be; in the metal shielding condition, the metallic sheets show no shielding effect as $k_{23}{}^{A} < k_c$, and show an excellent shielding effect as $k_{23}{}^{A}$ becomes close to and greater than k_c.

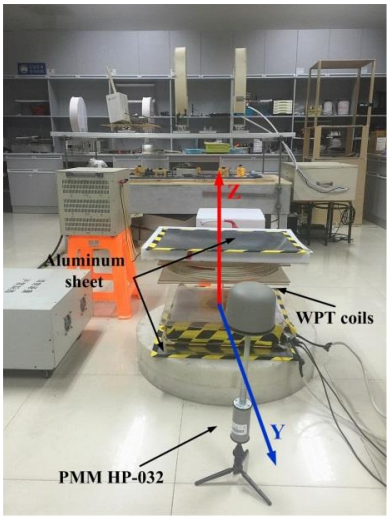

Figure 11. Experimental system.

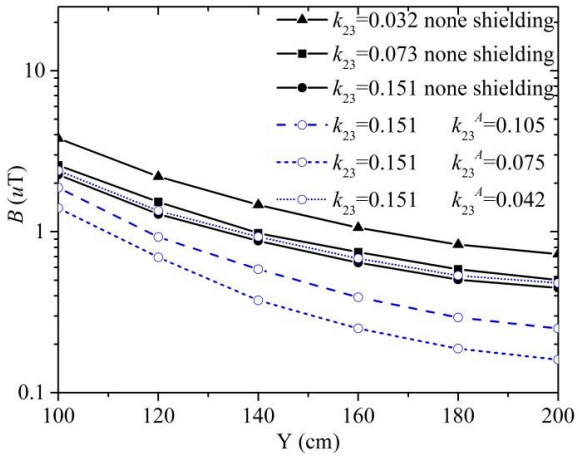

Figure 12. Experimental results of B_h under various coupling conditions.

4. Optimal Shielding Method

In the previous section, we discussed the metal shielding effectiveness under various coupling conditions, and demonstrated that an excellent shielding effect can be achieved together with acceptable electrical performance by the metals. However, this may also lead to the decline of the transmission power and distance. The analytic hierarchy process (AHP) is adopted to determine the optimal shielding method. For our ranking problem, we chose five shielding methods which have been studied as the alternatives: method 1: the coils distance and metal distance are assigned as d_{TR} = 30 cm, d_A = 10 cm; method 2: d_{TR} = 30 cm, d_A = 20 cm; method 3: d_{TR} = 30 cm, d_A = 30 cm; method 4: d_{TR} = 45 cm, d_A = 20 cm; method 5: d_{TR} = 45 cm, d_A = 30 cm. The shielding effectiveness, system efficiency, transmission power, transmission distance, and system size (total size including the metallic sheets) are determined to be the most important attributes affecting the ranking. The resulting decision tree that represents the hierarchical relationships between those elements is shown in Figure 13.

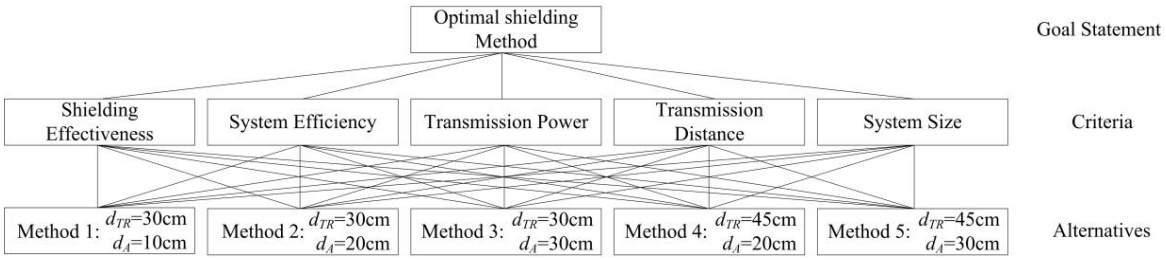

Figure 13. Analytic hierarchy process (AHP) decision tree with goal statement, criteria, and alternatives to be analyzed.

In our ranking problem, five shielding methods were assessed in terms of five criteria. The determination of the relative importance of each criterion toward the others was carried out through pairwise comparisons, for which experts expressed their preference by assigning a numerical value from 1 to 9 [19]. Results in Table 3 indicate that the criterion "shielding effectiveness" had the highest weight of 0.373, followed by "transmission power" and "transmission distance" which both had weights of 0.213. Therefore, "shielding effectiveness", "transmission power" and "transmission distance" should be the main concerns in ranking the shielding methods. "System efficiency" and "system size" had weights of 0.133 and 0.068, respectively. These results indicate that when ranking shielding methods, these two criteria should be of the least concern. The inconsistency value is determined as 0.019.

Table 3. Pairwise comparison matrix of criteria.

Criterion	Shielding Effectiveness	System Efficiency	Transmission Power	Transmission Distance	System Size	Relative Importance
Shielding effectiveness	1	3	2	2	4	0.373
System efficiency	1/3	1	1/2	1/2	3	0.133
Transmission power	1/2	2	1	1	3	0.213
Transmission distance	1/2	2	1	1	3	0.213
System size	1/4	1/3	1/3	1/3	1	0.068

Given the accepted criteria structure and the resulting importance weights obtained in Table 3, the research results in the previous section were subjected to pairwise comparisons in order to compare the shielding methods with respect to each criterion. Tables 4–8 show comparisons with shielding effectiveness, system efficiency, transmission power, transmission distance, and system size. The inconsistency value equals 0.018, 0.015, 0.022, 0, and 0.041, respectively.

Table 4. Pairwise comparison of alternatives according to "Shielding effectiveness" criteria.

Method	Method 1	Method 2	Method 3	Method 4	Method 5	Relative Importance
Method 1	1	2	3	5	7	0.434
Method 2	1/2	1	2	4	5	0.270
Method 3	1/3	1/2	1	3	4	0.172
Method 4	1/5	1/4	1/3	1	2	0.076
Method 5	1/7	1/5	1/4	1/2	1	0.048

Table 5. Pairwise comparison of alternatives according to "System efficiency" criteria.

Method	Method 1	Method 2	Method 3	Method 4	Method 5	Relative Importance
Method 1	1	1/4	1/5	1/2	1/3	0.062
Method 2	4	1	1/2	3	2	0.263
Method 3	5	2	1	4	3	0.419
Method 4	2	1/3	1/4	1	1/2	0.097
Method 5	3	1/2	1/3	2	1	0.160

Table 6. Pairwise comparison of alternatives according to "Transmission power" criteria.

Method	Method 1	Method 2	Method 3	Method 4	Method 5	Relative Importance
Method 1	1	3	4	1/3	1/2	0.173
Method 2	1/3	1	2	1/5	1/4	0.076
Method 3	1/4	1/2	1	1/6	1/5	0.051
Method 4	3	5	6	1	2	0.427
Method 5	2	4	5	1/2	1	0.273

Table 7. Pairwise comparison of alternatives according to "Transmission distance" criteria.

Method	Method 1	Method 2	Method 3	Method 4	Method 5	Relative Importance
Method 1	1	1	1	1/3	1/3	0.111
Method 2	1	1	1	1/3	1/3	0.111
Method 3	1	1	1	1/3	1/3	0.111
Method 4	3	3	3	1	1	0.333
Method 5	3	3	3	1	1	0.333

Table 8. Pairwise comparison of alternatives according to "System size" criteria.

Method	Method 1	Method 2	Method 3	Method 4	Method 5	Relative Importance
Method 1	1	3	5	6	8	0.510
Method 2	1/3	1	3	4	6	0.255
Method 3	1/5	1/3	1	2	4	0.119
Method 4	1/6	1/4	1/2	1	3	0.077
Method 5	1/8	1/6	1/4	1/3	1	0.039

Figure 14 provides a summary of the overall results of the comparative study. The first five value sets represent the local weights of five alternatives for each criterion and the last value set represents the final weights. Method 1 has the highest weight of 0.266, followed by method 4 with 0.208. They are followed by method 2, method 5, and method 3 with weights of 0.193, 0.171, and 0.162 respectively.

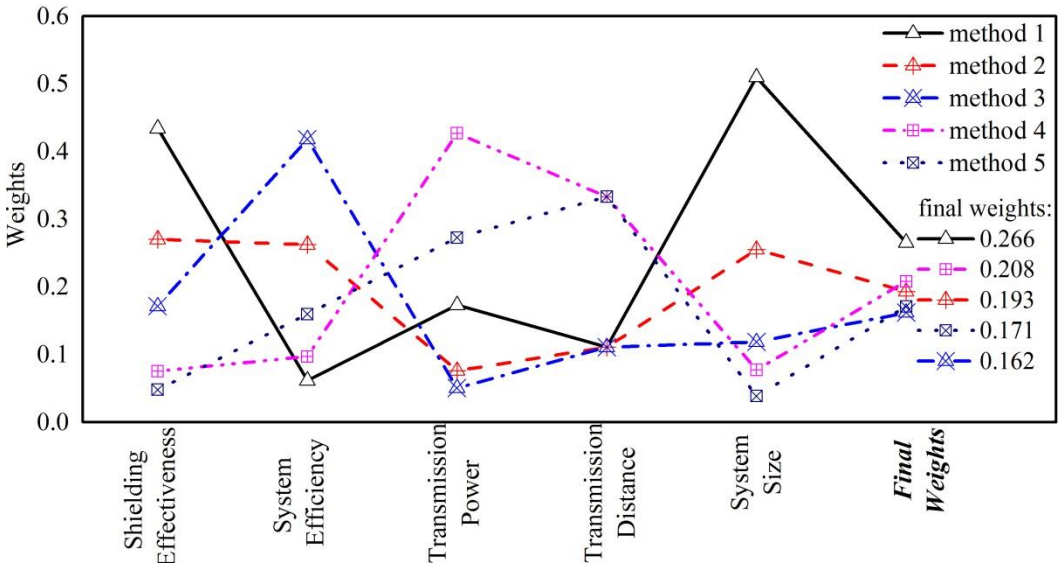

Figure 14. Weights of the shielding methods for each criterion and their final ranking.

5. Conclusions

In order to ensure that the magnetic field coupling WPT system is convenient to use and safely approachable, it is critical that the system complies with the relevant regulations without significant loss of electrical performance. In this paper, the magnetic field shielding method by metallic sheets in a WPT system is optimized. The simulation and measurement results shown here demonstrate that an excellent shielding effect can be achieved together with an acceptable electrical performance by obtaining the largest possible coupling coefficient of the coils within the allowable range and then reducing the value nearest to and no smaller than the critical coupling coefficient via geometric unbroken metallic sheets. The optimal magnetic field shielding method that considers the system efficiency, transmission power, transmission distance, and system size is also achieved using AHP. The conclusions in this paper will be useful for the magnetic field shielding design for high-power applications using magnetic field coupling WPT.

Acknowledgments: This work was supported in part by National Nature Science Youth Foundation of China (no. 51507032), Nature Science Youth Foundation of Jiangsu Province (no. BK20150617), State Grid Corporation Project of China, and Key Research and Development Planning Technique Project of Jiangsu Province (no. BE2015004-4).

Author Contributions: Feng Wen conceived and designed the study. He was also responsible for the simulations and experiments. This work was performed under the advisement and regular feedback from Xueliang Huang.

Conflicts of Interest: The authors declare no conflict of interest.

References

1. Campi, T.; Cruciani, S.; Palandrani, F.; de Santis, V.; Hirata, A.; Feliziani, M. Wireless Power Transfer Charging System for AIMDs and Pacemakers. *IEEE Trans. Microw. Theory Tech.* **2016**, *64*, 633–642. [CrossRef]
2. Ho, J.; Yeh, A.; Neofytou, E.; Kim, S. Wireless power transfer to deep-tissue microimplants. *Proc. Natl. Acad. Sci. USA* **2014**, *111*, 7974–7979. [CrossRef] [PubMed]
3. Miller, J.M.; Jones, P.T.; Li, J.M.; Onar, O.C. ORNL Experience and Challenges Facing Dynamic Wireless Power Charging of EV's. *IEEE Circuits Syst. Mag.* **2015**, *15*, 40–53. [CrossRef]
4. Kim, H.; Cho, J.; Ahn, S.; Kim, J. Suppression of leakage magnetic field from a wireless power transfer system using ferrimagnetic material and metallic shielding. In Proceedings of the IEEE International Symposium on Electromagnetic Compatibility (EMC), Pittsburgh, PA, USA, 6–10 August 2012; pp. 630–635.
5. Kim, S.; Jung, D.H.; Kim, J.J.; Bae, B.; Kong, S. Modeling of Electromagnetic Interference Shielding Materials in Wireless Power Transfer for Board-to-Board Level Interconnections. In Proceedings of the IEEE Wireless Power Transfer Conference, Jeju, Korea, 8–9 May 2014; pp. 273–276.

6. Mukherjee, S. Mitigation of Proximity to Metal for Magnetically Coupled Transponders by use of Resonant Loops. In Proceedings of the IEEE International Conference on RFID, Orlando, FL, USA, 8–10 April 2014; pp. 8–14.
7. Park, B.C.; Lee, J.H. Enhanced efficiency for wireless power transmission using an auxiliary loop on ferrite in metallic environment. *Electron. Lett.* **2015**, *51*, 2039–2040. [CrossRef]
8. Park, H.H.; Kwon, J.H.; Kwak, S.I.; Ahn, S. Effect of Air-Gap Between a Ferrite Plate and Metal Strips on Magnetic Shielding. *IEEE Trans. Magn.* **2015**, *51*, 1–4. [CrossRef]
9. Yu, X.F.; Skauli, T.B.; Skauli, S.; Sandhu, P.B. Wireless power transfer in the presence of metallic plates: Experimental Results. *AIP Adv.* **2013**, *3*. [CrossRef]
10. Ueda, N.; Fujimoto, M.; Hori, T.; Tabata, T.; Hori, S. Effect of metal plate on position error tolerance in wireless power transfer. In Proceedings of the 2012 International Symposium on Antennas and Propagation (ISAP), Nagoya, Japan, 29 October–2 November 2012; pp. 455–458.
11. Kudo, H.; Ogawa, K.; Oodachi, N.; Deguchi, N.; Shoki, H. Detection of a metal obstacle in wireless power transfer via magnetic resonance. In Proceedings of the IEEE 33rd International Telecommunications Energy Conference (INTELEC), Amsterdam, The Netherlands, 9–13 October 2011; pp. 1–6.
12. Albesa, J.; Gasulla, M. Inductive power transfer for autonomous sensors in presence of metallic structures. In Proceedings of the Instrumentation and Measurement Technology Conference (I2MTC), Graz, Austria, 13–16 May 2012; pp. 664–669.
13. Li, Q.; Chen, S.; Wang, W.; Hao, H.; Li, L. Improving the efficiency of magnetic coupling energy transfer by etching fractal patterns in the shielding metals. *Front. Inf. Technol. Electronic Eng.* **2016**, *17*, 74–82. [CrossRef]
14. Kim, H.; Song, C.; Kim, J.; Kim, J. Shielded coil structure suppressing leakage magnetic field from 100W-class wireless power transfer system with higher efficiency. In Proceedings of the Microwave Workshop Series on Innovative Wireless Power Transmission: Technologies, Systems, and Applications (IMWS), Kyoto, Japan, 10–11 May 2012; pp. 83–86.
15. Guidelines for Limiting Exposure to Time-varying Electric, Magnetic and Electromagnetic Fields pending confirmation(Up to 300 GHz). *Health Phys.* **1998**, *74*, 494–522.
16. Vecchia, P.; Hietanen, M.; Matthes, R.; Ahlbom, A.; Breitbart, E.; de Gruijl, F.R.; Feychting, M.; Green, A.; Jokela, K.; Lin, J.; et al. Guidelines for Limiting Exposure to Time-varying Electric and Magnetic Fields pending confirmation(1 Hz to 100 kHz). *Health Phys.* **2010**, *99*, 818–836.
17. Ma, J.; Sun, S.; Liu, C. Study of wireless power transfer link with metallic plates. In Proceedings of the IEEE MTT-S International Microwave Workshop Series on RF and Wireless Technologies for Biomedical and Healthcare Applications (IMWS-BIO), Singapore, Singapore, 9–11 December 2013; pp. 1–2.
18. Li, C.; Zhang, H.; Jiang, X. Parameters Optimization for Magnetic Resonance Coupling Wireless Power Transmission. *Sci.World J.* **2014**. [CrossRef] [PubMed]
19. Saaty, R.W. The analytic hierarchy process—what it is and how it is used. *Math. Model.* **1987**, *9*, 161–176. [CrossRef]